Revision_1

A single-crystal neutron diffraction study of wardite, $NaAl_3(PO_4)_2(OH)_4 \cdot 2H_2O$

G. Diego Gatta, Alessandro Guastoni, Oscar Fabelo and Maria Teresa Fernandez-Diaz

Running title: Neutron diffraction study of wardite

Corresponding author: G. Diego GATTA
Dipartimento di Scienze della Terra, Università degli Studi di Milano
Via Botticelli 23, I-20133 Milano, Italy
Tel. +39 02 503 15607, Fax +39 02 503 15597, E-Mail: diego.gatta@unimi.it

Manuscript submitted to Physics and Chemistry of Minerals

A single-crystal neutron diffraction study of wardite, $NaAl_3(PO_4)_2(OH)_4 \cdot 2H_2O$

G. Diego Gatta[1,2], Alessandro Guastoni[3], Oscar Fabelo[4] and Maria Teresa Fernandez-Diaz[4]

[1]Dipartimento di Scienze della Terra, Università degli Studi di Milano,
Via Botticelli 23, I-20133 Milano, Italy
[2] CNR-Istituto di Cristallografia, Via Amendola 122/O, I-70126 Bari, Italy
[3]Dipartmento di Geoscienze, Università degli Studi di Padova,
Via G. Gradenigo 6, I-35131, Padova, Italy
[4]Institut Laue-Langevin, 71 Avenue des Martyrs, F-38000 Grenoble, France

Abstract

The crystal structure and crystal chemistry of wardite, ideally $NaAl_3(PO_4)_2(OH)_4 \cdot 2H_2O$, was investigated by single-crystal neutron diffraction (data collected at 20 K) and electron microprobe analysis in wavelength-dispersive mode. The empirical formula of the sample used in this study is: $(Na_{0.91}Ca_{0.01})_{\Sigma=0.92}(Al_{2.97}Fe^{3+}_{0.05}Ti_{0.01})_{\Sigma=3.03}(P_{2.10}O_8)(OH)_4 \cdot 1.74H_2O$. The neutron diffraction data confirm that the crystal structure wardite can be described with a tetragonal symmetry (space group $P4_12_12$, $a = b = 7.0577(5)$ and $c = 19.0559(5)$ Å at 20 K) and consists of sheets made by edge-sharing Na-polyhedra and Al-octahedra along with vertex-sharing Al-octahedra, parallel to (001), connected by P-tetrahedra and H-bonds to form a (001) layer-type structure, which well explains the pronounced {001} cleavage of the wardite crystals. The present data show that four crystallographically independent H sites occur into the structure of wardite, two belonging to a H_2O molecule (*i.e.*, H1-O6-H2) and two forming hydroxyl groups (*i.e.*, O5-H3 and O7-H4). The location of the hydrogen atoms allow us to define the extensive network of H-bonds: the H-atoms belonging to the H_2O molecule form strong H-bonds, whereas both the H-atoms belonging to the two independent hydroxyl groups form weak interactions with bifurcated bonding schemes. As shown by the root-mean-square components of the displacement ellipsoids, oxygen and hydrogen atoms have slightly larger anisotropic displacement parameters if compared to the other sites (populated by P, Al and Na). The maximum ratio of the *max* and *min* root-mean-square components of the displacement ellipsoids is observed for the protons of the hydroxyl groups, which experience bifurcated H-bonding schemes. A comparative analysis of the crystal structure of wardite and fluorowardite is also provided.

Keywords: Wardite, phosphates, single-crystal neutron diffraction, crystal chemistry, hydrogen bonding.

Introduction

Wardite, ideally $NaAl_3(PO_4)_2(OH)_4 \cdot 2H_2O$, is a hydrous phosphate mineral discovered and described by Davison (1896). It was found in cavities in variscite nodules from the Clay Canyon deposit (near Fairfield) in Utah County (Davison 1896; Kampf et al. 2014). Wardite is a hydrothermal mineral, which occurs in phosphate-rich zones of granite pegmatites. After a series of experiments aimed to describe the chemical nature and the symmetry of the wardite crystals (*e.g.*, Hurlbut 1952; Heritsch 1955), its structure was solved by Fanfani et al. (1970), on the basis of single-crystal X-ray intensity data (collected by Weissenberg method with multiple-film integrated photographs) and using a crystal from the type locality. The authors described the structure of wardite in the space group $P4_12_12$, with unit-cell constants $a = b \sim 7.03$ Å, $c \sim 19.04$ Å (and $\alpha = \beta = \gamma = 90^o$). The wardite structure consists of sheets of Al- and Na-coordination polyhedra sharing vertices and edges. These sheets, parallel to (001), are connected to each other along the [001] direction by PO_4-tetrahedra (and H-bonds) (Fig. 1). The structure model reported by Fanfani et al. (1970) is consistent, in terms of bond distances and angles of the Na-, Al- and P-polyhedra. However, the quality of the data at that time did not allow the authors to locate the H sites, leaving open questions about configuration of the H_2O molecules and OH-groups and, as a consequence, about the H-bonding scheme in the wardite structure. Wardite contains up to 18 wt% of H_2O, therefore the H-content is not negligible. Based on electrostatic valences balance of the oxygen sites, Fanfani et al. (1970) suggested the potential occurrence of one independent H_2O-molecule and two independent hydroxyl-groups. A series of experiments on wardite have been performed by infrared and Raman spectroscopies (*e.g.*, Breitinger et al. 2004; Frost and Erickson 2005; Frost and Xi 2012). However, the full description of the active modes was hindered by the lack of a structure model in which the H sites positions, their vibrational regimes and the H-bonding scheme were known.

More recently, Kampf et al. (2014) reported the occurrence of fluorowardite, ideally $NaAl_3(PO_4)_2(OH)_2F_2 \cdot 2H_2O$. The structure was solved and described on the basis of a single-crystal X-ray structure refinement; a comparative description of the crystal structure of wardite and fluorowardite was provided.

In the framework of a long-term project on the crystal-chemistry of hydrous phosphates (*e.g.*, Gatta et al. 2013a, 2013b, 2014a, 2014b, 2015), we have reinvestigated the crystal structure and crystal

chemistry of wardite by single-crystal neutron diffraction and electron microprobe analysis in wavelength-dispersive mode (EPMA–WDS), in order to provide: *i*) the reliable location of the proton sites and the real topological configuration of the OH-groups and H_2O molecules, for a full description of the atomic relationship via the H-bonds; *ii*) the anisotropic displacement parameters of all the atomic sites, H-sites included. To carry out this objective, single-crystal neutron diffraction data were collected at low temperature (20 K) in order to reduce the thermal displacement of the H-sites.

Sample description and occurrence

The sample of wardite used in this study belongs to the collection of the Museum of Mineralogy of the University of Padova (catalogue number MM18662). The hand specimen is a group of pseudo-octahedral gem-quality crystals, formed by nearly equant tetragonal di-pyramids, striated perpendicular to [001], with pale blue-green colour and up to 1 cm in length. The larger crystals are transparent and vitreous. The specimen was collected at the Rapid Creek area, Canada. The Rapid Creek is a remote region in the north-eastern Yukon Territory, but it represents a remarkable deposit of uncommon and rare phosphate mineral species. Since the early 70s, this area became, among mineralogists and mineral collectors, one of the most important sources for fine minerals like arrojadite group minerals, augelite, collinsite, gorceixite, goyazite, kryzhanovskite, lazulite, wardite and whiteite (Robinson et al. 1992). This is also the type locality for several new iron-, magnesium-, manganese- and barium-phosphate minerals, including arrojadite-(KNa) (Moore et al. 1981), barićite (Sturman and Mandarino 1976), garyansellite (Sturman and Dunn 1984), gormanite (Sturman et al. 1981), kulanite (Mandarino and Sturman 1976), penikisite (Mandarino et al. 1977) and rapidcreekite (Roberts et al. 1986), a calcium, hydrate sulphate-carbonate.

Young and Roberston (1984) published a geological description of the Rapid Creek area, which is characterized by deposits of siderite and phosphatic ironstone embedded in shales and thick sequences of turbidite sandstones, named Blow River Formation, deposited during the early to mid-Cretaceous. The phosphatic iron formation is composed of phosphate-siderite grains, detrital quartz and skeletal fragments in a matrix of sideritic mudstone. Most of the phosphate grains are not composed by apatite but of rare phosphate minerals including arrojadite, gormanite and satterlyite. At Rapid Creek, well-crystallized phosphates occur within set of rigid fracture which cross-cut the Blow River Formation, where a typical fracture-filling mineral assemblage is related to the composition of the hosting rocks (Robertson 1982). Robertson (1982) identified four major mineral assemblages: 1) Ba-rich set of fractures cross-cutting conglomerates, 2) Ca-rich fractures cross-cutting mudstones, 3) Fe-Mg-Mn rich set of fractures cross-cutting sandstones, and 4) Na-rich set of

fractures cross-cutting phosphatic sandstones. The wardite sample used for this study is associate with spheroidal aggregates of millimetric greenish-bluish gormanite and rhombohedral brown vitreous millimetric crystals of siderite, probably related to the type 3 set of fractures as reported by Robertson (1982).

There is no geological evidence of the presence of an igneous activity in the area; the host rock is a sedimentary iron-rich formation. Fluid inclusion studies indicate that the sequence of crystallization of phosphates at Rapid Creek occurred between 180-200° C, with quartz, lazulite and arrojadite, which represent the first minerals to crystallize, whilst wardite occurs as late stage phosphate. Except for minor illite and chlorite observed in the shales, no lawsonite, laumontite or pyrophillite occur in the sedimentary rocks at Rapid Creek (Robertson 1982). For such a reason, the fracture-filling minerals were probably formed in the uppermost diagenesis to the lowermost range of regional metamorphism (Robinson et al. 1992).

Experimental methods

Chemical composition of the wardite used in this study was obtained using a CAMECA SX-50 electron microprobe equipped with four wavelength-dispersive spectrometers and one energy-dispersive spectrometer at the laboratory of microanalysis of the Institute for Geosciences and Earth Resources of CNR (Padova). The operating conditions were 20 kV accelerating voltage, 5 nA beam current and 10 μm beam diameter. Counting times were 10 s at the peak and 5 s at the background for major elements, and 20 to 100 s at peak and background for minor elements. X-ray counts were converted into oxide weight percentages using the PAP correction program (Pouchou and Pichoir 1991). Calibration was performed using natural and synthetic international standards, in part supplied by Cameca and in part kindly provided by the Smithsonian National Museum of Natural History (Smithsonian Microbeam Standards). The following reference materials, lines, and analysing crystals were used: wollastonite (Si*K*α-TAP); diopside (Ca*K*α-PET); albite (Na*K*α-TAP); fluorapatite (P*K*α-TAP); corundum (Al*K*α-TAP); $MnTiO_3$ (Ti*K*α-PET); FeO (Fe*K*α-LIF); $MnTiO_3$ (Mn*K*α-LIF); orthoclase (K*K*α-PET); AsGa (As*L*α, TAP). The elements K and As (and even F) were sought but resulted below the experimental detection limits (*i.e.*, less than 0.03 wt%). Minor evidence of sample dehydration, under the electron beam, were observed. Further details pertaining to the microprobe chemical analysis are given in Table 1.

Neutron diffraction data were collected on the four-circle diffractometer D19 at ILL (Grenoble, France) with Cu(331)-monochromated radiation (take-off angle $2\theta_M$ = 70°), providing neutrons with a wavelength of 0.9460 Å. The sample was glued on a ϕ = 0.5 mm vanadium pin

and placed on a close-circuit displex device operated at 20.0(5) K (Archer and Lehmann 1986). The measurement strategy consists of omega (ω) scans of 64 or 79° with steps of 0.07° at different χ and φ positions. A total of 25 ω-scans were collected to complete almost half-Ewald sphere. The Multi-Detector Acquisition Data Software (MAD) from ILL was used for data collection. The unit-cell determination was done by using PFIND and DIRAX programs (Duisenberg 1992). The integration of the raw data and refinement of the UB-matrix, including the off-sets, were done using RETREAT and RAFD19 programs, respectively (Wilkinson et al. 1988). The lattice was found to be metrically tetragonal, and the reflections conditions agreed with the space group $P4_12_12$, as previously reported by Fanfani et al. (1970). A total of 20478 reflections were integrated, out of which 3109 were unique reflections (Laue group 4/*mmm*, $R_{int} = 0.0411$). The absorption correction, mainly due to the hydrogen content of the sample (*ca*. 0.132 mm^{-1}), was carried out using D19abs program (Matthewman et al. 1982). Further details pertaining to the data collection strategy are listed in Table 2 and in Gatta et al. (2018a).

Anisotropic crystal-structure refinement based on the neutron intensity data was done in the space group $P4_12_12$ using the SHELXL-2014 software (Sheldrick 2008, 2014), starting from the structure model of Fanfani et al. (1970), without any H atom. The neutron scattering lengths of Na, Al, Fe, P, O and H were taken from Sears (1986). Secondary isotropic extinction effect was corrected according to the formalism of Larson (1967), as implemented in the SHELXL package. Convergence was rapidly reached after the first cycles of refinement with a series of intense negative residual peaks in the final difference-Fourier map of the nuclear density (Fig. 2). Minima in the difference-Fourier maps of the nuclear density showed no evidence of positional or dynamic disorder (Fig. 2). Further cycles of refinement were done with H sites assigned to these peaks (as H has a negative neutron scattering length). At the end of the refinement (with $R_1(F) = 0.0219$ for 3106 reflections with $F_O > 4\sigma(F_O)$ and 129 refined parameters), all variable parameters converged with all the principal mean-square atomic displacement parameters positive, including those for the H sites. The variance-covariance matrix showed no significant correlation among the refined variables. Further details pertaining to structure refinement strategy are given in Table 2. Coordinates of the atomic sites and displacement parameters are listed in Tables 3 and 4; selected interatomic distances and angles are given in Table 5.

Results and Discussion

The EPMA–WDS analysis of the wardite sample used in this study confirms the general findings previously reported in the literature: the ideal formula of this mineral is

$NaAl_3(PO_4)_2(OH)_4 \cdot 2H_2O$; Na is replaced by a very modest fraction of Ca, P (in tetrahedral coordination) is replaced by a low fraction of Si; Al (in octahedral configuration) is replaced by Fe, Mn and Ti (Table 1). Previous experimental findings confirmed that iron occurs as Fe^{3+} in wardite (Vassilikou-Dova 1993). The empirical formula of wardite used in this study is: $(Na_{0.91}Ca_{0.01})_{\Sigma=0.92}(Al_{2.97}Fe^{3+}_{0.05}Ti_{0.01})_{\Sigma=3.03}(P_{2.10}O_8)(OH)_4 \cdot 1.74H_2O$ (Table 1).

The neutron structure refinement of this study, based on intensity data collected at 20 K, is consistent with the general structural model previously obtained by Fanfani et al. (1970), based on single-crystal X-ray intensity data collected at room conditions: wardite structure consists of sheets made by edge-sharing Na-polyhedra (with coordination number = 8) and Al-octahedra along with vertex-sharing Al-octahedra, parallel to (001), connected by P-tetrahedra and H-bonds to form a (001) layer-type structure, which well explains the pronounced {001} cleavage of the wardite crystals (Fig. 1, Table 5). Accordingly, strong structural homologies occur between the crystal structure of wardite and fluorowardite (ideally $NaAl_3(PO_4)_2(OH)_2F_2 \cdot 2H_2O$, Kampf et al. 2014). Our data show that in wardite the P-tetrahedron is almost regular (with $\Delta(P\text{-}O)_{max} \sim 0.02$ Å, *i.e.*, the difference between the longest and the shortest bond distances), whereas the two independent Al-octahedra are slightly distorted ($\Delta(Al1\text{-}O)_{max} \sim 0.15$ Å, $\Delta(Al2\text{-}O)_{max} \sim 0.03$ Å). Four crystallographically independent H sites occur into the structure of wardite (namely H1-H4, Table 3). In particular:

- H1 and H2 form a H_2O molecule with the O6 site (oxygen site shared by adjacent Na-polyhedron and Al-octahedron, Fig. 1), with H1-O6-H2 = 110.0(1)°, O6-H1* = 1.013 Å and O6-H2* = 0.996 Å (* corrected for *riding motion effect*, Table 5);
- H3 forms an hydroxyl group with the O5 site (as bridging oxygen site shared by adjacent Al-octahedra, Fig. 1), with O5-H3* = 0.986 Å (Table 5);
- H4 forms an hydroxyl group with the O7 site (as bridging oxygen site shared by adjacent Al-octahedra, Fig. 1), with O7-H4* = 0.989 Å (Table 5).

The H-bonding scheme in the structure of wardite is now well defined:

- The H1 site is H-bonded to the O2 site, with O6-H1···O2 = 174.4(1)° and H1···O2 = 1.617(1) Å (Fig. 1, Table 5);
- The H2 site is H-bonded to the O5 site, with O6-H2···O5 = 160.1(1)° and H2···O5 = 1.913(1) Å (Fig. 1, Table 5);
- The H3 site shows a bifurcated bonding scheme with O5-H3···O1 = 139.9(1)° and H3···O1 = 2.556(1) Å, and O5-H3···O6 = 148.5(1)° and H3···O6 = 2.347(1) Å (Fig. 1, Table 5);

- The H4 site also shows a bifurcated bonding scheme with O7-H4···O3 = 160.5(1)° and H4···O3 = 2.447(1) Å, and O7-H4···O4 = 137.9(1)° and H4···O4 = 2.449(1) Å (Fig. 1, Table 5).

Whereas the H2-O6-H2 molecule experiences two strong H-bonds, as corroborated by the bonding geometry, the two hydroxyl groups show relatively weak interactions (Table 5). The H1-O6-H2 angle (Table 5) is still in the range of the observed H-O-H angles in solid-state materials (Chiari and Ferraris 1982; Steiner 1998 and references therein; Gatta et al. 2008, 2012, 2018b; Lotti et al. 2018). The hydrogen bonds of the H_2O molecule show O-H···O angles ≥ 160° (Table 5), with a configuration energetically favorable (*i.e.*, approaching linearity, Steiner 1998); the bifurcated H-bonding configuration of the two independent hydroxyl groups leads to a bonding geometry energetically more costly. In fluorowardite, one of the two independent hydroxyl groups is replaced by fluorine, but the H_2O content is virtually identical to that of wardite: the replacement $OH^- \rightarrow F^-$ is possible, without any significant rearrangement of the structure, because of the (very) weak H-bonds generated by the hydroxyl group. The H-bonding scheme in the structure of wardite here described is compatible with the findings based on vibrational spectroscopies (*e.g.*, Breitinger et al. 2004; Frost and Erickson 2005; Frost and Xi 2012). A more robust description of the active IR vibrational modes, dictated by the H-bonds, can now be delivered on the basis of the experimental findings of this study.

As shown by the root-mean-square components of the displacement ellipsoids, oxygen and hydrogen atoms have slightly larger anisotropic displacement parameters if compared to the other sites (populated by P, Al and Na). The maximum ratio of the *max* and *min* root-mean-square components of the displacement ellipsoids is observed for the protons of the hydroxyl groups (*i.e.*, O5-H3 and O7-H4, Table 4), which experience bifurcated H-bonding schemes.

The neutron structure refinement does not show evidence of partial site occupancy of the H_2O group (Table 3). In this light, the molecular H_2O fraction of the calculated unit formula (*i.e.*, 1.74 molecules *p.f.u.*, Table 1), in which the H_2O wt% was assumed considering $(OH)_{\Sigma=4}$, is likely underestimated: according to the neutron structure refinement, wardite contains 2.0 molecules *p.f.u.*. The underestimation of the (total) water content could be related with the replacement of OH-group by fluorine, as observed in fluorowardite, and neither X-ray nor neutron diffraction are able to distinguish unambiguously between O and F as their scattering factors/lengths are quite similar. The EPMA–WDS analysis of the wardite used in this study does not show a significant content of fluorine; however, evidence of dehydration under the electron beam were observed during the EPMA-WDS analysis.

Acknowledgements

The authors thank the Institut Laue-Langevin (Grenoble, France), for the allocation of the beamtime and the Institute for Geosciences and Earth Resources of CNR (Padova) for the microprobe analysis of wardite. Two anonymous reviewers and the Editor, M. Rieder, are thanked. This manuscript is dedicated to Pier Francesco Zanazzi (b. 1939), professor of Mineralogy and Crystallography at the University of Perugia (Italy), who solved and refined the structure of wardite with Luca Fanfani and Antonio Nunzi in the 1970, on the occasion of his 80th birthday.

References

Archer J, Lehmann MS (1986) A simple adjustable mount for a two-stage cryorefrigerator on an Eulerian cradle. J Appl Crystallogr 19:456-459.

Breitinger DK, Belz H-H, Hajba L, Komlosi V, Mink J, Brehm G, Colognesi D, Parker SF, Schwab RG (2004) Combined vibrational spectra of natural wardite. J Molec Struct 706:95–99.

Busing WR, Levy HA (1964) The effect of thermal motion on the estimation of bond lengths from diffraction measurements. Acta Crystallogr 17:142-146.

Chiari G, Ferraris G (1982) The water molecules in crystalline hydrates studied by neutron diffraction. Acta Crystallogr B38:2331–2341.

Davison JM (1896) Wardite: a new hydrous basic phosphate of alumina. Am J Science 2:154–155.

Duisenberg AJM (1992) Indexing in single-crystal diffractometry with an obstinate list of reflections. J Appl Crystallogr 25:92-96.

Fanfani L, Nunzi A, Zanazzi PF (1970) The crystal structure of wardite. Mineral Mag 37:598-605.

Frost RL, Erickson KL (2005) Near-infrared spectroscopic study of selected hydrated hydroxylated phosphates. Spectrochim Acta A61:45-50.

Frost RL, Xi YA (2012) Vibrational spectroscopic study of the phosphate mineral Wardite $NaAl_3(PO_4)_2(OH)_4{\cdot}2H_2O$. Spectrochim Acta A93:155-163.

Gatta GD, Rotiroti N, McIntyre GJ, Guastoni A, Nestola F (2008) New insights into the crystal chemistry of epididymite and eudidymite from Malosa, Malawi: a single-crystal neutron diffraction study. Am Mineral 93:1158–1165.

Gatta GD, McIntyre GJ, Swanson GJ, Jacobsen SD (2012) Minerals in cement chemistry: a single-crystal neutron diffraction and Raman spectroscopic study of thaumasite, $Ca_3Si(OH)_6(CO_3)(SO_4){\cdot}12H_2O$. Am Mineral l97:1060–1069.

Gatta GD, Vignola P, Meven M, Rinaldi R (2013a) Neutron diffraction in gemology: Single-crystal diffraction study of brazilianite, $NaAl_3(PO_4)_2(OH)_4$. Am Mineral 98:1624–1630.

Gatta GD, Nénert G, Vignola P (2013b) Coexisting hydroxyl groups and H_2O molecules in minerals: A single-crystal neutron diffraction study of eosphorite, $MnAlPO_4(OH)_2 \bullet H_2O$. Am Mineral 98:1297–1301.

Gatta GD, Jacobsen SD, Vignola P, McIntyre GJ, Guastella G, Abate LF (2014a) Single-crystal neutron diffraction and Raman spectroscopic study of hydroxylherderite, $CaBePO_4(OH,F)$. Mineral Mag, 78, 723-737.

Gatta GD, Vignola P, Meven M (2014b) On the complex H-bonding network in paravauxite, $Fe^{2+}Al_2(PO_4)_2(OH)_2 \cdot 8H_2O$: A single-crystal neutron diffraction study. Mineral Mag 78:841–850.

Gatta GD, Redhammer GJ, Vignola P, Meven M, McIntyre GJ (2015) Single-crystal neutron diffraction and Mössbauer spectroscopic study of hureaulite, $(Mn,Fe)_5(PO_4)_2(HPO_4)_2(H_2O)_4$. Eur J Mineral 28:93-103.

Gatta GD, Fabelo Rosa OR, Fernandez-Diaz MT (2018a) On the crystal chemistry of the wardite, $NaAl_3(PO_4)_2(OH)_4$ x $2H_2O$. Institut Laue-Langevin (ILL, Grenoble): doi:10.5291/ILL-DATA.5-11-430.

Gatta GD, Hålenius U, Bosi F, Cañadillas-Delgado L, Fernandez-Diaz MT (2018b) Minerals in cement chemistry: a single-crystal neutron diffraction study of ettringite, $Ca_6Al_2(SO_4)_3(OH)_{12} \cdot 27H_2O$. Am Mineral (*in press,* DOI: https://doi.org/10.2138/am-2019-6783).

Heritsch H (1955) Die Raumgruppe von Wardit. Tschermaks Min Petr Mitt 5: 246-251.

Hurlbut CS (1952) Wardite from beryl mountain, New Hampshire. Am Mineral 37:849-852.

Kampf AR, Adams PM, Housley RM, Rossman GR (2014) Fluorowardite, $NaAl_3(PO_4)_2(OH)_2F_2 \cdot 2H_2O$, the fluorine analogue of wardite from the Silver Coin mine, Valmy, Nevada. Am Mineral 99:804-810.

Larson AC (1967) Inclusion of secondary extinction in least-squares calculations. Acta Crystallogr 23:664 – 665.

Lotti P, Gatta GD, Demitri N, Guastella G, Rizzato S, Ortenzi MA, Magrini F, Comboni D, Guastoni A, Fernandez-Diaz MT (2017) Crystal-chemistry and temperature behavior of the natural hydrous borate colemanite, a mineral commodity of boron. Phys Chem Minerals 45:405–422.

Mandarino JA, Sturman BD (1976) Kulanite, a new barium iron aluminum phosphate from the Yukon Territory, Canada. Can Mineral 14:127-131.

Mandarino JA, Sturman BD, Corlett MI (1977) Penikisite, the magnesium analogue of kulanite, from the Yukon Territory, Canada. Can Mineral 15:393-395.

Matthewman JC, Thompson P, Brown PJ (1982) The Cambridge Crystallography Subroutine Library. J Appl Crystallogr 15:167-171.

Moore PB, Araki T, Merlino S, Mellini M, Zanazzi PF (1981) The arrojadite-dickinsonite series, $KNa_4Ca(Fe,Mn)^{2+}_{14}Al(OH)_2(PO_4)_{12}$: crystal structure and crystal chemistry. Am Mineral 66:1034–1049.

Pouchou J-L, Pichoir F (1991) Quantitative analysis of homogeneous or stratified microvolumes applying the method "PAP". In: Heinrich KFJ, Newbury DE (eds) Electron probe quantitation. Plenum Press, New York, 31-75.

Robertson BT (1982) Occurrence of epigenetic phosphate minerals in a phosphatic iron formation, Yukon Territory. Can Mineral 20:177-187.

Roberts AC, Ansell HG, Jonasson IR, Grice JD, Ramik RA (1986) Rapidcreekite, a new hydrated calcium sulfate-carbonate from the Rapid Creek area, Yukon Territory. Can Mineral 24:51-54.

Robinson GW, Van Velthuizen J, Ansell HG, Sturman BD (1992) Mineralogy of the Rapid Creek and Big Fish River area, Yukon Territory. Min Rec 23:1-47

Sears VF (1986) Neutron Scattering Lengths and Cross-Sections. In K. Sköld and D.L. Price, Eds., Neutron Scattering, Methods of Experimental Physics, Vol. 23A, 521-550. Academic Press, New York.

Sheldrick GM (2008) A short history of SHELX. Acta Crystallogr A64:112-122.

Sheldrick GM (2014) SHELXL-2014. Programs for crystal structure determination and refinement. University of Göttingen, Germany.

Steiner T (1998) Opening and narrowing of the water H-O-H angle by hydrogen-bonding effects: Re-inspection of neutron diffraction data. Acta Crystallogr B54:464-470.

Sturman BD, Mandarino JA (1976) Baricite, the magnesium analogue of vivianite, from the Yukon Territory, Canada. Can Mineral 14:403-406.

Sturman BD, Dunn PJ (1984) Garyansellite, a new mineral from Yukon Territory. Am Mineral 69:207-209.

Sturman BD, Mandarino JA, Mrose ME, Dunn PJ (1981) Gormanite, $Fe^{2+}_3Al_4(PO_4)_4(OH)_6{\cdot}2H_2O$, the ferrous analogue of souzalite, and new data for souzalite. Can Mineral 19:381-387.

Vassilikou-Dova AB (1993) An EPR study of trivalent iron in wardite. Appl Magn Reson 5:25-29.

Wilkinson C, Khamis HW, Stansfield RFD, McIntyre GJ (1988) Integration of single-crystal reflections using area multidetectors. J Appl Crystallogr 21:471-478.

Young FG, Robertson BT (1984) The Rapid Creek Formation: An Albian Flysch-Related Phosphatic Iron Formation in Northern Yukon Territory. In: The Mesozoic of Middle North America, D.F. Stott and D.J. Glass, eds. Canadian Society of Petroleum Geologists Memoir 9, 361-372.

368 Table 1. EPMA-WDS chemical analysis of wardite from Rapid Creek, Yukon, Canada. Average composition based on

369 14 point analysis.

370

Oxides	***Wt%***	***e.s.d.***
Na_2O	7.02	6.29-7.43
Al_2O_3	37.84	36.53-39.31
SiO_2	0.03	0.01-0.06
P_2O_5	37.28	36.65-37.80
CaO	0.12	0.07-0.17
TiO_2	0.10	0.04-0.15
MnO	0.02	0.01-0.06
Fe_2O_3	0.93	0.50-1.45
H_2O	16.85	
Total	100.19	

Elements	***a.p.f.u.***
Na	0.91
Ca	0.01
Al	2.97
Fe^{3+}	0.05
Ti	0.01
Mn	0.00
P	2.10
H^+	7.48

Notes:

- Analysis calculated on the basis of 14 anions
- Fixed $(OH)_{\Sigma=4}$
- Fe_2O_3 calculated from FeO_{tot} obtained by microprobe analysis

The empirical formula of wardite results:
$(Na_{0.91}Ca_{0.01})_{\Sigma=0.92}(Al_{2.97}Fe^{3+}_{0.05}Ti_{0.01})_{\Sigma=3.03}(P_{2.10}O_8)(OH)_4 \cdot 1.74H_2O$

371

372

373

374

375

376

377

378

379

380

381

382

383

Table 2. Details of neutron data collection and refinement of wardite.

T (K)	20.0(5)
Crystal shape	Prism
Crystal volume (mm)	2 x 2 x 3
Crystal colour	Pale blue-green
Unit-cell parameters	$a = b =$ 7.0577(5) Å
	$c =$ 19.0559(5) Å
Chemical formula	$NaAl_3(PO_4)_2(OH)_4 \bullet 2H_2O$
Space Group	$P4_12_12$
Z	4
Radiation type	neutron
Wavelength (Å)	0.94602
Diffractometer	D19 four circle -ILL
Data-collection method	ω-scans
Max. 2θ (°)	122.25
	$-12 \le h \le +12$
	$-12 \le k \le +7$
	$-34 \le l \le +35$
Measured reflections	20478
Unique reflections	3109
Unique reflections with $F_o > 4\sigma(F_o)$	3106
Refined parameters	129
Extinction coeff.	0.0060(7)
R_{int}	0.0411
R_σ	0.0214
R_1 *(F)* with $F_o > 4\sigma(F_o)$	0.0219
R_1 *(F)* for all reflections	0.0221
$wR_2(F^2)$	0.0518
GooF	1.195
Residuals (fm/Å^3)	-0.68/+0.68

Note: Statistical parameters according to the Shelxl-2014 definition (Sheldrick 2008, 2014).

412 Table 3. Refined fractional atomic coordinates and equivalent/isotropic displacement factors (Å^2), based on the
413 neutron structure refinement. U_{eq} is defined as one third of the trace of the orthogonalised U_{ij} tensor. All the sites show
414 *s.o.fs* of 100%.
415
416

Site	*x/a*	*y/b*	*z/c*	U_{eq}
P	0.14076(7)	0.36564(7)	0.34911(2)	0.00306(7)
Al1	0.39588(11)	0.10694(11)	0.25770(4)	0.0029(1)
Al2	0.10298(11)	0.10298(11)	0	0.0031(1)
Na	0.37371(11)	0.37371(11)	0.5	0.0063(1)
O1	-0.03785(7)	0.42506(7)	0.30966(3)	0.00483(7)
O2	0.29995(7)	0.51346(7)	0.33752(2)	0.00443(7)
O3	0.20513(7)	0.17351(7)	0.32071(3)	0.00497(7)
O4	0.09981(7)	0.35105(7)	0.42774(2)	0.00469(7)
O5	0.13341(7)	0.35260(7)	-0.03932(2)	0.00453(7)
O6	0.18718(7)	0.03209(7)	0.19138(3)	0.00585(7)
O7	0.40821(7)	0.34989(7)	0.21653(2)	0.00480(7)
H1	0.1264(2)	0.1027(2)	0.15197(6)	0.0178(2)
H2	0.1584(2)	-0.1030(2)	0.18760(7)	0.0199(2)
H3	0.0827(2)	0.3519(2)	-0.0860(1)	0.0232(2)
H4	0.5094(2)	0.3408(2)	0.18255(7)	0.0215(2)

417

Table 4. Refined displacement parameters (Å^2) in the expression: $-2\pi^2[(ha^*)^2U_{11} + \ldots + 2hka^*b^*U_{12} + \ldots + 2klb^*c^*U_{23}]$ and root-mean-square displacement amplitude (*RMS*, Å), based on the neutron structure refinement of wardite.

	U_{11}	U_{22}	U_{33}	U_{12}	U_{13}	U_{23}
P	0.0030(2)	0.0030(2)	0.0032(1)	0.0001(1)	-0.0001(1)	-0.0002(1)
Al1	0.0030(2)	0.0028(2)	0.0031(2)	0.0001(2)	0.0000(2)	0.0002(2)
Al2	0.0027(2)	0.0027(2)	0.0037(3)	-0.0002(2)	0.0002(2)	-0.0002(2)
Na	0.0062(2)	0.0062(2)	0.0067(3)	0.0001(3)	0.0000(2)	0.0000(2)
O1	0.0038(1)	0.0055(2)	0.0052(1)	0.0003(1)	-0.0008(1)	0.0012(1)
O2	0.0044(2)	0.0044(2)	0.0046(1)	-0.0012(1)	0.0001(1)	-0.0001(1)
O3	0.0054(2)	0.0038(2)	0.0058(2)	0.0004(1)	0.0010(1)	-0.0008(1)
O4	0.0046(1)	0.0058(2)	0.0037(1)	0.0003(1)	0.0003(1)	0.0002(1)
O5	0.0052(1)	0.0037(1)	0.0047(1)	0.0001(1)	-0.0003(1)	0.0001(1)
O6	0.0063(2)	0.0055(2)	0.0058(1)	-0.0003(1)	-0.0014(1)	0.0003(1)
O7	0.0051(1)	0.0038(1)	0.0055(1)	0.0001(1)	0.0007(1)	-0.0001(1)
H1	0.0201(4)	0.0182(4)	0.0151(3)	0.0020(3)	-0.0030(3)	0.0033(3)
H2	0.0241(5)	0.0119(3)	0.0236(5)	-0.0036(3)	-0.0035(4)	-0.0004(3)
H3	0.0365(7)	0.0197(5)	0.0133(4)	0.0020(5)	-0.0106(4)	-0.0014(3)
H4	0.0225(5)	0.0193(5)	0.0227(5)	0.0015(4)	0.0128(4)	0.0009(4)

	RMS-min	*RMS-mid*	*RMS-max*	*max/min*
P	0.05405	0.05430	0.05762	1.066
Al1	0.05175	0.05428	0.05644	1.091
Al2	0.05029	0.05230	0.06180	1.229
Na	0.07756	0.07937	0.08188	1.056
O1	0.05591	0.06932	0.08093	1.448
O2	0.05612	0.06734	0.07493	1.335
O3	0.05677	0.07116	0.08144	1.435
O4	0.05978	0.06772	0.07694	1.287
O5	0.06112	0.06750	0.07285	1.192
O6	0.06802	0.07356	0.08673	1.275
O7	0.06180	0.06797	0.07727	1.250
H1	0.10714	0.14260	0.14685	1.371
H2	0.10362	0.14534	0.16661	1.608
H3	0.09549	0.13966	0.20222	2.118
H4	0.09881	0.13837	0.18875	1.910

Table 5. Relevant bond distances (Å) and angles (°) based on the neutron structure refinement.

P - O1	1.5265(7)	O1 - P - O2	110.10(4)	O5-H3	0.959(1)
P - O2	1.5490(7)	O1 – P - O3	108.34(4)	O5-H3*	0.986
P - O3	1.5291(7)	O1 - P - O4	110.18(4)	O5-H3···O1	139.9(1)
P - O4	1.5295(5)	O2 - P - O3	109.35(4)	O5···O1	3.347(1)
		O2 - P - O4	108.79(4)	H3···O1	2.556(1)
Al1 - O1	1.8661(9)	O3 - P - O4	110.07(4)	O5-H3···O6	148.5(1)
Al1 - O3	1.8641(9)			O5···O6	3.205(1)
Al1 - O4	1.9165(9)	O1 - Al1 - O3	176.37(5)	H3···O6	2.347(1)
Al1 - O5	1.9047(9)	O1 - Al1 - O4	88.48(4)		
Al1 - O6	2.0114(9)	O1 - Al1 - O5	92.57(4)	O6-H1	0.998(1)
Al1 - O7	1.8876(9)	O1 - Al1 - O6	89.72(4)	O6-H1*	1.013
		O1 - Al1 - O7	85.43(4)	O6-H1···O2	174.4(1)
Al2 - O2 x 2	1.9105(6)	O3 - Al1 - O4	95.16(4)	O6···O2	2.613(1)
Al2 - O5 x 2	1.9265(9)	O3 - Al1 - O5	87.44(4)	H1···O2	1.617(1)
Al2 - O7 x 2	1.8983(9)	O3 - Al1 - O6	86.68(4)		
		O3 - Al1 - O7	94.13(4)	O6-H2	0.978(1)
Na - O4 x 2	2.3788(8)	O4 - Al1 - O5	91.39(4)	O6-H2*	0.996
Na - O1 x 2	2.4756(7)	O4 - Al1 - O6	173.67(4)	O6-H2···O5	160.1(1)
Na - O6 x 2	2.5659(10)	O4 - Al1 - O7	95.26(4)	O6···O5	2.852(1)
Na - O3 x 2	2.7199(8)	O5 - Al1 - O6	82.63(4)	H2···O5	1.913(1)
		O5 - Al1 - O7	173.00(5)	H1-O6-H2	110.0(1)
		O6 - Al1 - O7	90.64(4)		
				O7-H4	0.966(1)
		O2 - Al2 - O2	177.74(5)	O7-H4*	0.989
		O2 - Al2 - O5	92.78(4)	O7-H4···O3	160.5(1)
		O2 - Al2 - O5	85.58(3)	O7···O3	3.373(1)
		O2 - Al2 - O7	89.83(4)	H4···O3	2.447(1)
		O2 - Al2 - O7	91.74(3)	O7-H4···O4	137.9(1)
		O5 - Al2 - O5	86.98(4)	O7···O4	3.231(1)
		O5 - Al2 - O7	90.70(3)	H4···O4	2.449(1)
		O5 - Al2 - O7	174.75(4)		
		O7 - Al2 - O7	91.98(4)		

* Bond distance corrected for "riding motion" following Busing and Levy (1964)

Figure 1. Two views of the crystal structure of wardite based on the neutron structure refinement of this study (intensity data collected at 20 K). Displacement ellipsoid probability factor: 50%.

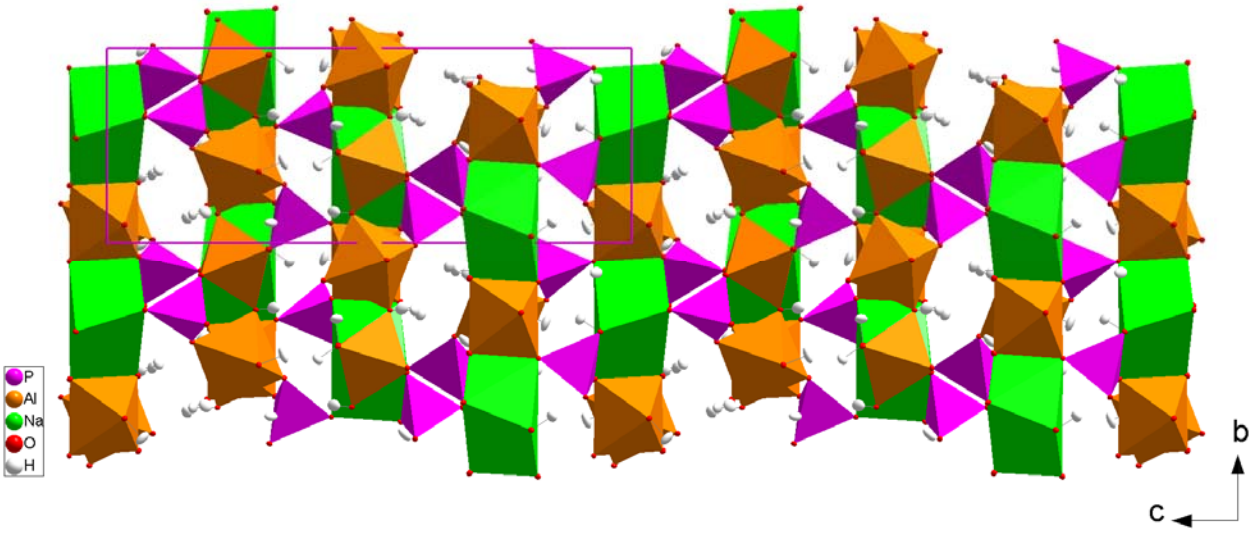

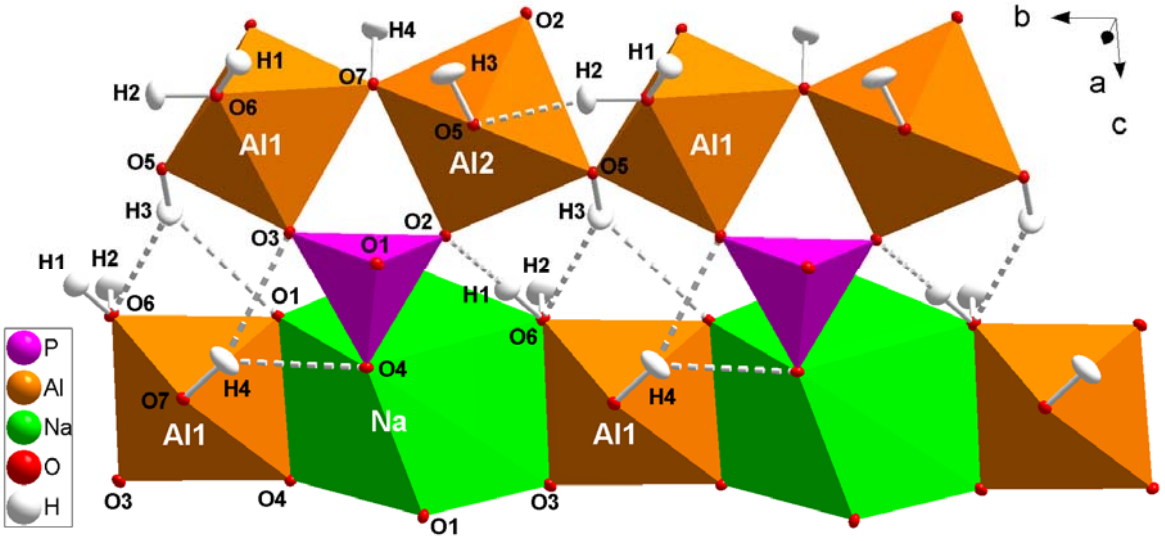

Figure 2. Difference-Fourier maps of the nuclear density (*xy* sections, *x* horizontal; $z \sim 0.15$ for the H1 map, $z \sim 0.19$ for the H2 map, $z \sim -0.09$ for the H3 map, $z \sim 0.18$ for the H4 map) calculated with coefficients *Fo-Fc* and phased by *Fc*. The *Fc* were calculated from a structural model without the H sites. Minima, ascribable to the missing H sites (as H has negative neutron scattering length) are visible. Color bar unit: fm/Å^3.

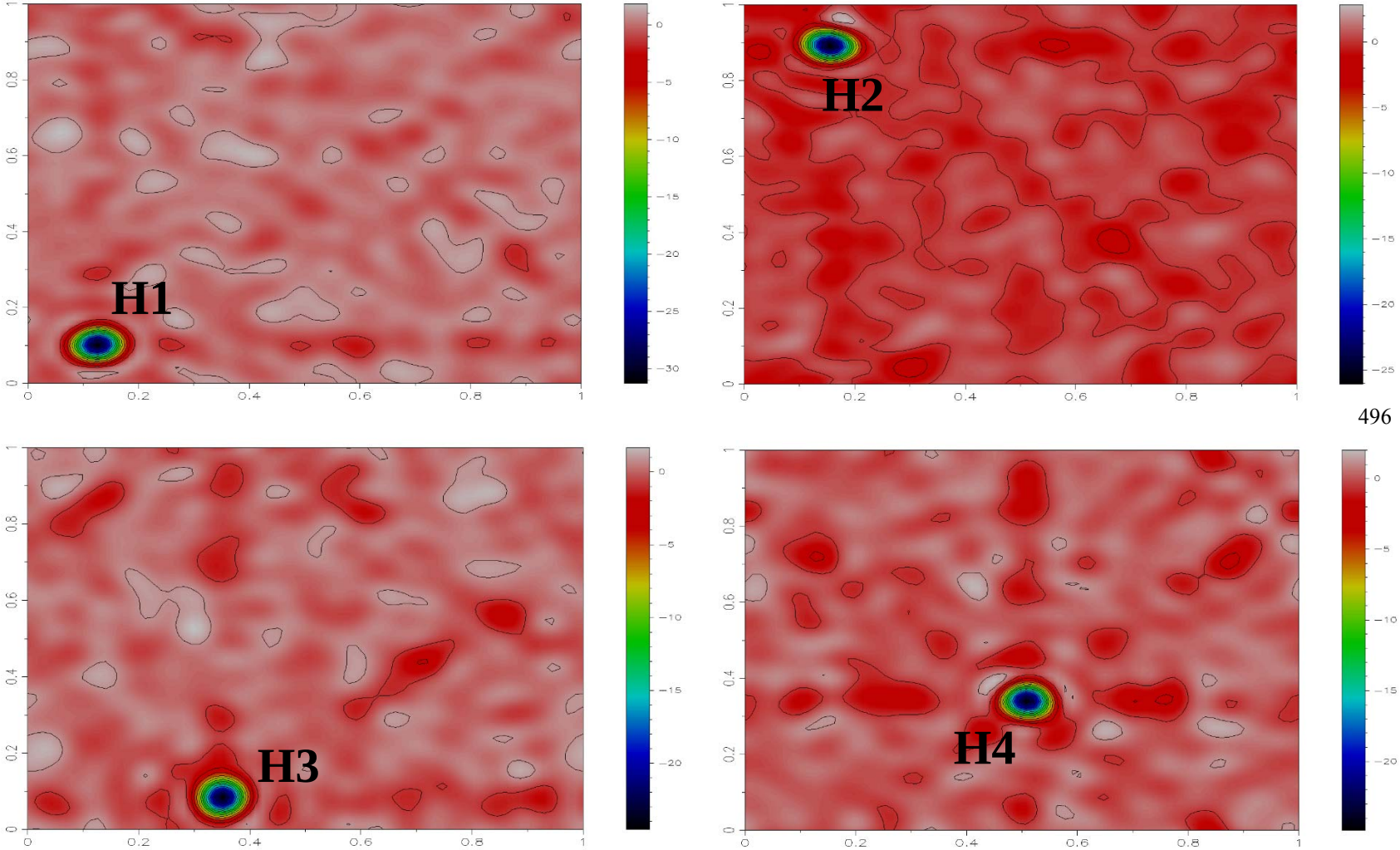

510